Postprint of: Ryndzionek R., Michna M., Ronkowski M., Rouchon J.: Chosen Analysis Results Of The Prototype Multicell Piezoelectric Motor, IEEE-ASME TRANSACTIONS ON MECHATRONICS, Vol. 23, iss. 5 (2018), pp. 2178-2185,
DOI: 10.1109/TMECH.2018.2865619

Chosen Analysis Results Of The Prototype Multicell Piezoelectric Motor

Roland Ryndzionek, Michał Michna, *Senior Member, IEEE,* Mieczysław Ronkowski, *Member, IEEE,* and Jean-Francois Rouchon

***Abstract*—This paper presents the design, modeling and tests of the prototype multicell piezoelectric motor (MPM). A new concept of the electromechanical structure of the considered prototype is based on three rotating-mode actuators. The electromechanical structure of each actuator has been considered as an independent one - referred to as a "single cell" (single actuator). Combined three resonant actuators generate three traveling waves which as a result improve the stability and performance of the MPM. The results of research carried out using analytical, simulation and experimental methods cover the torque vs. speed characteristics of the prototype MPM.**

***Index Terms*—Piezoelectricity, Piezoelectric transducers, Traveling wave devices, Piezoelectric resonators, Simulation, Piezoelectric actuators, Piezoelectric motors**

I. Introduction

ADVANCED mechatronic motion systems are characterized by increasing integration of motors, actuators and sensors with a coupling mechanism. Significant progress in the field of materials engineering gives an opportunity to develop electromechanical structures that feature flexible implementation and motion control [1]–[4]. Generally, electromechanical structures are developed using electromagnetic and piezoelectric systems. The physical (and technological) limits of electromagnetic structures have already been reached. In contrast, the physical limits are far from being reached in the field of piezoelectric structures [5], [6].

Piezoelectricity is widely used in industrial sectors such as the production and detection of sound, generation of high voltages, electronic frequency generation, microbalances, driving an ultrasonic nozzle and ultrafine focusing of optical assemblies [3]. It can be found useful in everyday life activities, such as acting as an ignition source for lighters. Moreover, the piezoelectric materials have electro-magneto-elastic coupling properties that can be used to build electromechanical transducers, motors and actuators [7]–[9].

The piezoelectric motors are relatively new compared to electromagnetic motors. They are characterized by high force density, multi-degree motion control, and perfect immunity to magnetic fields. Other authors have pointed out that piezoelectric motors have high potential in specialized and advanced applications [10]. However, piezoelectric motors have some disadvantages. These motors need a special high voltage and high frequency power sources. Their principle of operation is based on friction, which is related to the fast wear of layers (contact points) between the stator and rotor, high operating temperatures and the necessity to disperse heat.

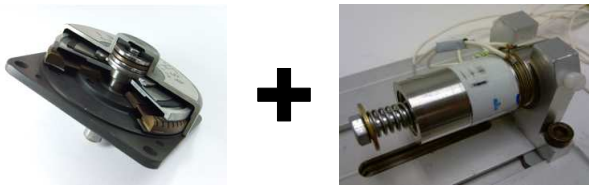

Fig. 1. The ultrasonic traveling wave motor [15] and rotating mode motor [16].

In this paper, the authors described the process of designing and analyzing the parameters (performance) of a new multicell piezoelectric motor (MPM) prototype. Finite element analysis was used to compute the resonance frequency and to select the appropriate structure for the single actuator. The MPM prototype was built and then tested. Torque vs. speed characteristics were measured and compared with the results obtained from analytical modeling. The main purpose of this paper is the presentation of the design, modeling, fabrication and test of the novel MPM prototype.

The paper is organized as follows: in chapter II the concept of the novel MPM is described. Chapter III presents the FEM model of the MPM which is used to determine the resonance frequencies and the stress in counter-mass structures. The analytical model of the MPM is developed in Chapter IV to determine torque vs. speed characteristics. Chapter V presents the experimental results of the MPM prototype and compares them with theoretical torque vs. speed characteristics. Finally, the conclusions are presented in Chapter VI.

The research has been carried out in cooperation with the Laboratory on Plasma and Conversion of Energy (LAPLACE) in Toulouse [11], and the Gdansk University of Technology, Faculty of Electrical and Control Engineering, Department Of Power Electronics and Electrical Machines [12].

II. The concept of MPM

The concept of a new piezoelectric motor [13], [14] is based on a combined topology of the traveling wave motor and the rotating-mode motor (Fig. 1).

This motor is referred to as a "multicell piezoelectric motor" because the topology for each rotating-mode motor can be considered as an independent structure - referred to as a "single cell". A proper mix of the performance of the three rotating-mode actuators will generate three traveling waves. This topology combines the advantages of both motors with

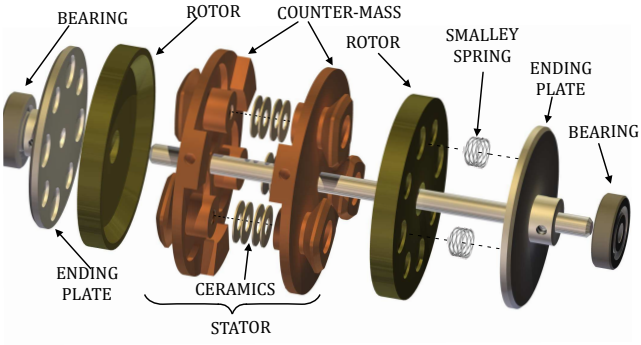

Fig. 2. The virtual model prototype of the multicell piezoelectric motor.

the following features: higher driving force on the rotor, higher speed and torque, high resonant frequency of each cell, prestressed symmetrical structure and high blocking torque [5], [17], [18]. Moreover, the multicell topology supports the stability of the motor structure. The motor has a few times less weight than an electromagnetic machine of the same volume (the weight of the MPM stator is 300 g). Finally, the motor should work in an ultrasonic frequency range (higher than 20 kHz) because it is inaudible for the human ear.

In the process of the MPM prototype creation, important aspects have been taken into account, for example: active parts - piezoelectric ceramics, counter-mass and rotors material. The prototype MPM has been determined by the dimensions of the piezoelectric ceramics - hard lead-zirconate-titanate PZT ceramic (PZT 189 by Quartz & Silice manufacturer, Tab. I). Moreover, the PZT materials offer low mechanical and dielectric losses and obtain high electroacoustic performances. The chosen ceramics have the following dimensions: external diameter – 12.5 mm, internal diameter – 5 mm, thickness – 1 mm. The ceramics have been sectored and polarized in LAPLACE Laboratory [11]. The polarization process included:

- laser sectorization of the ceramics, dividing it into two areas of the same size,
- ceramic polarization, the ceramics are placed in a container of dielectric oil between the two electrodes of the power supply, the voltage value is +/- 1.0 kV, the process lasts a minimum of 60 minutes,
- verification of polarization, the value of d_{33} coefficient of the ceramic is verified,
- capacity calculation.

In order to check if the polarization was properly done, it was necessary to use a device to measure the piezoelectric constant (d_{33}) – "Model ZJ-4B series quasi-static d_{33} meter". ". It should be noted that the measured results were not equal for all piezoceramics. The average value of the constant d_{33} was 350×10^{-12} C/N.

The selected piezoelectric material parameters used in FEM software and the analytical model are as follows:

TABLE I
QUARTZ & SILICE PZT189 MANUFACTURER PROPERTIES.

Parameter	Symbol	Model Value
Dielectric constants	ε_{33}^{T}	1150
Coupling factors	k_{31}	0.32
	k_{33}	0.65
	k_{15}	0.46
Piezo charge coefficients [10-12 C/N]	d_{31}	-108
	d_{33}	-240
Quality factor	Q_m	1000
Density [kg/m^3]	ϱ	7600

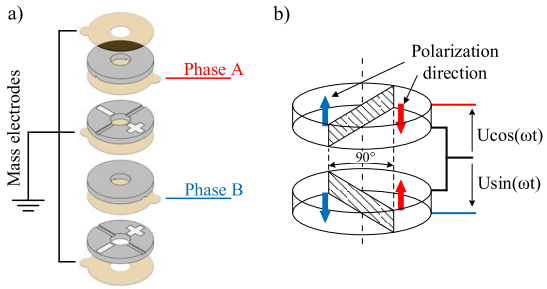

Fig. 3. Piezoceramics arrangement in single actuator of MPM.

$$(e) = \begin{pmatrix} 0 & 0 & -6.17 \\ 0 & 0 & -6.17 \\ 0 & 0 & 13.90 \\ 0 & 0 & 0 \\ 0 & 12.86 & 0 \\ 18.86 & 0 & 0 \end{pmatrix}$$

$$(c^E) = \begin{pmatrix} 154 & 82 & 81 & 0 & 0 & 0 \\ & 154 & 81 & 0 & 0 & 0 \\ & & 130 & 0 & 0 & 0 \\ & & & 36 & 0 & 0 \\ & & & & 46 & 0 \\ & & & & & 46 \end{pmatrix}$$

$$(\varepsilon^S) = \begin{pmatrix} 1142 & 0 & 0 \\ 0 & 1142 & 0 \\ 0 & 0 & 668 \end{pmatrix} \varepsilon_0$$

The stator consists of two pairs of piezoceramics and counter-masses with three rotating-mode actuators (Fig. 2). This supports a more stable structure than in a single rotating-mode motor structure.

Different methods are employed to generate a traveling wave. In general, a stator is build using an annular piezoelectric plate element. This element is sectored into halves and covered by electrodes (Fig. 3a). Each sector is polarized in opposite directions. The piezoelectric ceramic half with positive polarization will expand when positive voltage is applied. At the same time, the half with negative polarization will shrink. The two pairs of piezoelectric ceramics are orthogonally placed, so it is possible to generate two bending modes (Fig. 3b).

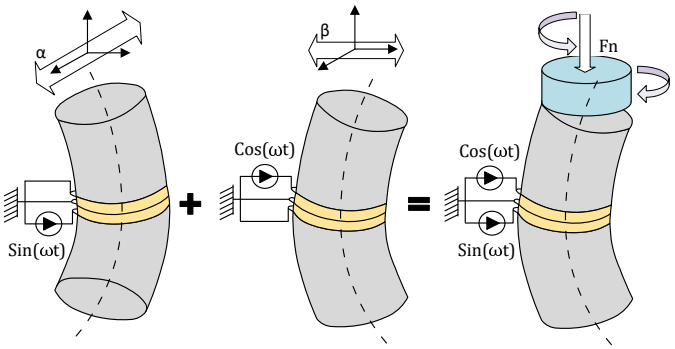

Fig. 4. Operation principle of a single actuator in MPM [19].

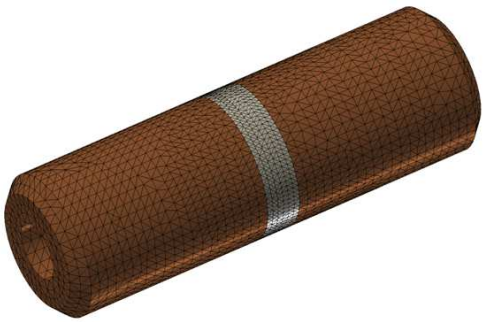

Fig. 5. The finite element mesh of the single actuator.

To generate a traveling wave on the surface of each single resonance actuator, two sinusoidal voltages sources with phase shift are necessary (Fig. 4).

To increase the vibration amplitude generated by ceramic, counter-masses are placed on both sides. The symmetrical structure of the stator allows for the use of two rotors on the same motor axis which increases output torque. To obtain better operating conditions, the rotor is not fixed directly on the shaft. The special Smalley springs enable an adjustment the rotor to the stator (Fig. 2). Crest-to-crest wave springs with shim ends, a 10 mm diameter and a height of 8 mm have been chosen - model CMS14-L4. Smalley wave springs offer the advantage of saving space when used to replace coil springs [20].

III. FEM MODELING

In the first step of the motor development , its finite element models have been built and subsequent simulations have been carried out.

The FEM models has been used for two purposes: determining the resonance frequencies of a single actuator and to simulate the stress in a counter-mass structure caused by rotor pressure force. The analysis of the resonance frequencies of a single transducer was carried out using Autodesk Inventor software. The results of the analysis have been used to determine the overall dimensions of a single actuator to obtain the required resonance frequency. The model in the FEM software consisted of a set of piezoceramic tiles and two symmetrically placed counter-masses (Fig. 5).

The mesh settings have been adjusted to obtain an even distribution of finite elements. The parameter named ”average elements size” was set to 0.05 and the remaining values were set to their default values (minimum element size, grading factor and maximum turn angle).

The finite element mesh of the actuator is presented in Fig. 5.

The mesh of the single actuator was generated automatically by the software and was then manually adjusted (in piezoceramic plate regions) to finally reached 86 000 elements (tetrahedron) and 140 000 nodes. Moreover, the FEM model allows for the study of the stator behavior in the tangential or radial direction. The results of a modal analysis have shown that several modes were observed in a 10 kHz - 100 kHz

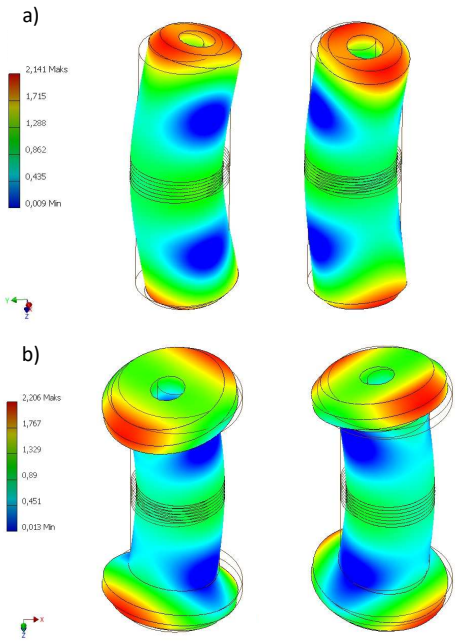

Fig. 6. The deformation principle in the single actuator of the first and second FEM model.

frequency range. Each actuator has two bending modes and one is the respiration mode. These modes remain strongly uncoupled in terms of frequency and low coupling coefficients. However, the stator excitation on its functional mode does not lead to excitation of the other modes. Several actuator FEM models have been developed that differ in shape and dimensions and are then simulated by FEM software.

As stated above, the stator consists of two counter-masses with three rotating mode actuators. All actuators are connected and oriented by 120° from each other. This design helps to keep the solid structure and provides satisfactory integration of the mechanical parts. In all simulation cases , aluminum counter-mass was treated as isotropic and material parameters were set as: density $\rho = 2720\,\mathrm{kg/m^3}$, Young's modulus $Y = 69\,\mathrm{GPa}$ and Poissons ratio $\sigma = 0.33$.

The first (Fig. 6a) and second (Fig. 6b) models have been developed to determine the overall dimensions of the single actuator to obtain the required resonance frequency. In Fig. 6a the following parameters were chosen: length of the single

TABLE II
THE RESONANCE FREQUENCIES OF SINGLE MPM ACTUATOR OBTAINED FROM FEM SIMULATIONS.

No.	Model Fig. 6a	Model Fig. 6b
1	29.34 kHz	25.93 kHz
2	29.36 kHz	25.95 kHz
3	40.12 kHz	27.07 kHz

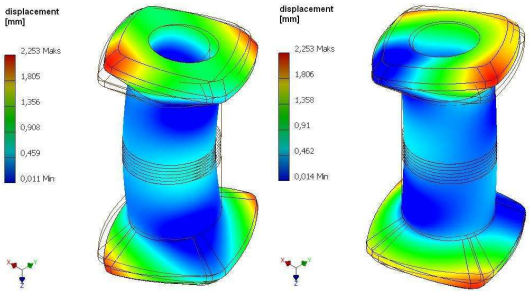

Fig. 7. The deformation principle in a single actuator of the final design.

actuator including thickness of four piezoceramics - 40 mm, external diameter – 12.5 mm, internal diameter – 5 mm. In Fig. 6b length of the single actuator including thickness of four piezoceramics – 36 mm, external diameter and internal diameter are the same

The shape with a hat in Fig. 6b creates a larger contact surface between the stator and rotor. The resonance frequencies obtained from FEM simulations are shown in Table II.

To get the required frequency, the length of a single actuator with four piezoelectric ceramics has been set up at 34 mm. The final geometry of a single actuator in counter-mass is presented in fig. 7. The actuators hat has been expanded. Thus, the rotor stator contact zone is much larger.

The simulations have shown three resonances: 25.61 kHz, 25.64 kHz and 25.68 kHz. Summarizing, the resonance frequencies are satisfactory due to being within the ultrasonic range.

The second issue that was solved using the FEM software was the counter-mass structure strength analysis. To simulate the stress in a counter-mass structure caused by rotor pressure force, Autodesk Multiphysics was used. Due to the complex structure of the entire multicell piezoelectric motor, the static stress analysis has been limited only to one part – counter-mass (Fig. 8). The counter-mass was made of aluminum and such a material was defined and used in the FEM software. To generate the highest quality mesh with the fewest elements the "*bricks and tetrahedral*" mesh type was chosen. This means that the model consists mainly of 8-node elements. The aspect ratio of the solid elements is controlled by a "*maximum aspect ratio*" parameter which was set to its default value. It means that it is calculated based on the surface mesh density. The "*varies rate*" parameter controls how the mesh size transitions from smaller areas of the model to larger areas. The transition rate was set to 1.2 and the quality to 100. The resulting mesh of counter-mass is shown in Fig. 8.

The rotor pressure force (120 N) was defined at each actuator as a constant valued vector acting along the Z-axis.

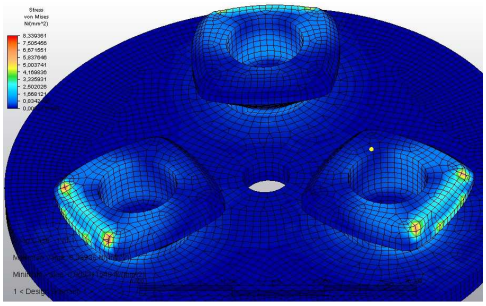

Fig. 8. The full view of counter-mass with three rotating mode actuators.

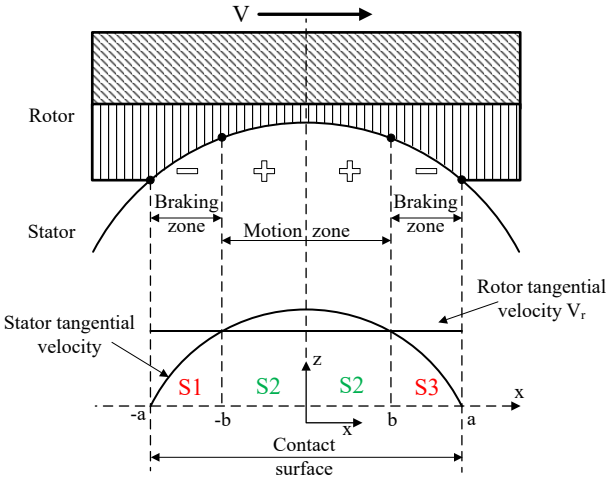

Fig. 9. Contact zone between stator and rotor of the MPM.

The results of the analysis were used to check the strength of the counter-mass with three rotating mode actuators.

IV. ANALITYCAL MODELING

The main purpose of the analytical modeling was to determine the torque vs. speed characteristics of MPM and to compare them with the experimental results of the MPM prototype.

In [19], analytical modelling of the piezoelectric rotating-mode motor has been presented. The model is based on an equivalent electric circuit and gives electro-mechanical characteristics by using the geometrical and electromechanical parameters. In the authors approach, due to specific features of the MPM prototype, the modeling method [19] has been modified. In the modified model accurate electromechanical parameters which describe material properties (e.g. density, Poisson ratio) were used. However, simplified geometric parameters were used due to the complex structure of the MPM.

Its implementation allows for the modeling of each actuator of MPM separately and also reduces the minimum number of the kinematic variables [9], [19].

First of all, the friction zones should be considered. Assuming that the friction coefficient is constant, it can be concluded that the contact surface is divided into three zones – S2 as a motion zone $\langle -b, +b \rangle$, S1 and S3 as a braking zones – $\langle -a, -b \rangle$ and $(+b, +a\rangle$ respectively (Fig. 9). These surfaces represent the tangential friction, which is in fact the image

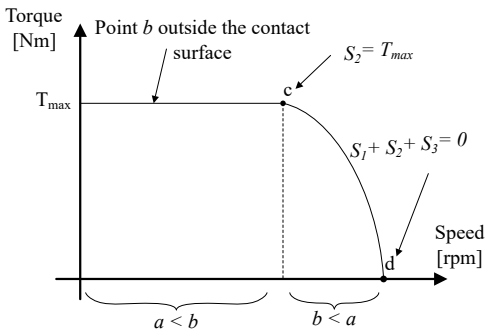

Fig. 10. Theoretical torque vs. speed characteristic of a rotating-mode piezoelectric.

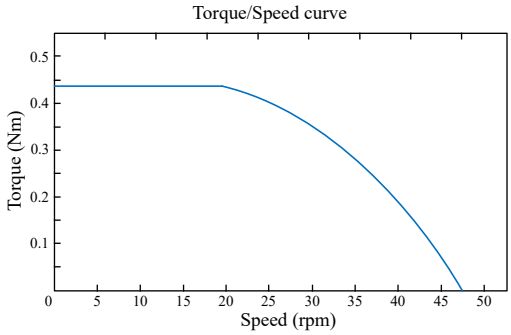

Fig. 11. Torque vs. speed characteristic of the MPM.

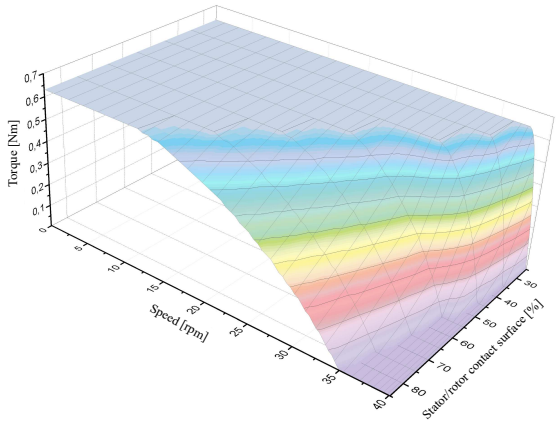

Fig. 12. Torque vs. speed 3D plot characteristics in terms of the stator/rotor contact surface.

of the torque. The surface between the *-b* and *+b* points corresponds to the rotor speed. Point *d* on the torque vs. speed characteristic (Fig. 10) corresponds to the rotor speed, when the torque is zero.

Due to the increase of the load, the drive zone S2 increases, so the torque increases as well. The maximum torque is at point *c* because the surface S2 reaches its maximum value (S1 = S3 = 0) (Fig. 10). If the motor load is constant, then the *b* point will be moved outside of the contact surface. Therefore, the curve torque vs. speed is still linear, because the motion zone cannot be larger than the contact zone. The theoretical torque value for the case, when $b < a$, can be calculated using the following formula [19]:

$$T = 2\mu r \left(\int_0^b p(x)\omega dx - \int_b^a p(x)\omega dx \right) \tag{1}$$

where: p – pressure distribution, x – dummy variable.

The maximum torque for $b > a$ was calculated from:

$$T_{max} = \frac{\pi}{2}\mu A \omega r P_0 \tag{2}$$

where:

$$p = P_0 \left(1 - \left(\frac{x}{A} \right)^2 \right)^{\frac{1}{2}} \tag{3}$$

μ – friction coefficient,
A – length of the contact zone,
ω – width of the contact zone,
r – radius of the actuator,
P_0 – pressure of average value.

This structure is symmetrical, thus the output torque becomes two times larger:

$$T_{max} = 2\mu r F_n \tag{4}$$

The maximum velocity of the motor at the point where $b = a$ was calculated by this formula:

$$\Omega = \frac{U_0 cos\left(\frac{A}{r}\right)\omega}{r} \tag{5}$$

where: U_0 – vibration amplitude in radial vibration.

Based on the calculations from formulas (1)–(5), the torque vs. speed characteristic has been determined (Fig. 11). The total torque of the MPM has been approximated using the following method: the torque value computed for the single actuator has been multiplied by three (corresponding to three resonance actuators). The most important parameters are: the blocking torque – 0.44 Nm and the maximum speed – 47 rpm.

Fig. 12 shows the torque vs. speed characteristic in terms of the stator/rotor contact surface. With higher contact surface, the characteristic becomes more ”smooth”. However, the efficiency of the motor becomes lower due to the heat generated by friction.

The appropriate selection of the contact surface, depends on the shape of the actuator structure and the required torque.

V. Experimental results of the MPM prototype

The MPM prototype has a complex structure and atypical shape of its resonance actuators. The counter-mass was manufactured using a 3D printer. The material used for the production of the counter-mass is aluminum because of its high resonance frequencies and satisfactory mechanical losses. The prototype counter-mass has been produced by the French company INITIAL [21]. The diameter of the stator is 50 mm and each actuator has a diameter of 12.5 mm. The surface around the actuator is 1 mm thick, and the diameter of the surface is 8 mm. The external diameter is 60 mm, the internal diameter is 10 mm and the inclination angle is 45° (Fig. 13). The rotor was manufactured using steel. The rotational motion

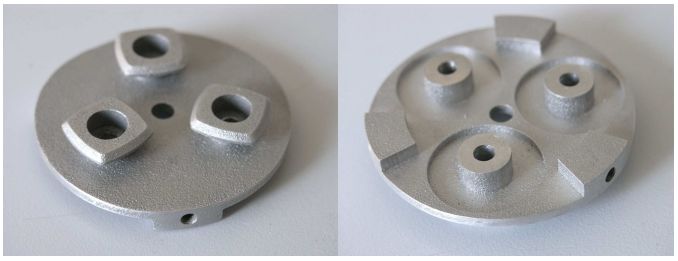

Fig. 13. The outside and inside view of the prototype counter-mass.

of the rotor is transmitted to the shaft by ”Smalley” springs [20] and two plates.

At the beginning, the resonance frequency of each actuator of MPM was measured. The crucial goal was to obtain the same frequencies for each actuator. The measured resonance frequency was near 22 kHz for all three actuators. It should also be pointed out that the resonance frequency depends on the force applied by the screw and the tightening torque as well. The measurements of resonance frequency are presented in Fig. 14.

In the next step of the measurements, the dSPACE laboratory stand was used to measure the torque vs. speed characteristics of the MPM prototype (Fig. 15), because it offers Hardware-In-the-Loop control.

The full assembly of the MPM prototype has been presented in Fig. 16. The housing has been manufactured by a 3D printer using Nylatron GF30-66.

The dSpace control panel allows for control of the output voltage from 0 V to 1000 V and a frequency range around 50 kHz. The measurements were done for 400 V and a frequency of 22 kHz. For these parameters of power supply, the MPM vibration amplitude was the highest and reached the optimal values suggested by the manufacturer of the piezoceramic. Any further voltage increase results in increasing the vibration which can cause fast degradation of the ceramic. The torque was measured on the rotor shaft using a Torque-Transducer T20WN. The speed was calculated from the number of revolutions made at the measured time. Measurements were made for distinctive points of the torque vs. speed curve and are presented in Fig. 17. The differences between the analytical calculations and the measurements results are caused by the use of a simplified analytical model of the MPM prototype. The analytical model does not take into account the changing of the friction coefficient and the quality of contact between the stator and the rotor. Increase stators and rotors temperature causes a non-linear change in the friction coefficient value which is not considered in the used analytical model. The quality of the contact between the stator and rotor changes because of different pressures being applied by each ”Smalley” spring on the rotor. However, the comparison of theoretical and measurement characteristics is satisfactory and can provide useful perspectives for further MPM study and design.

For MPM prototype by optimizing the mechanical structure and selecting an appropriate pressing force on the rotor, the following measurements have been determined: the maximum

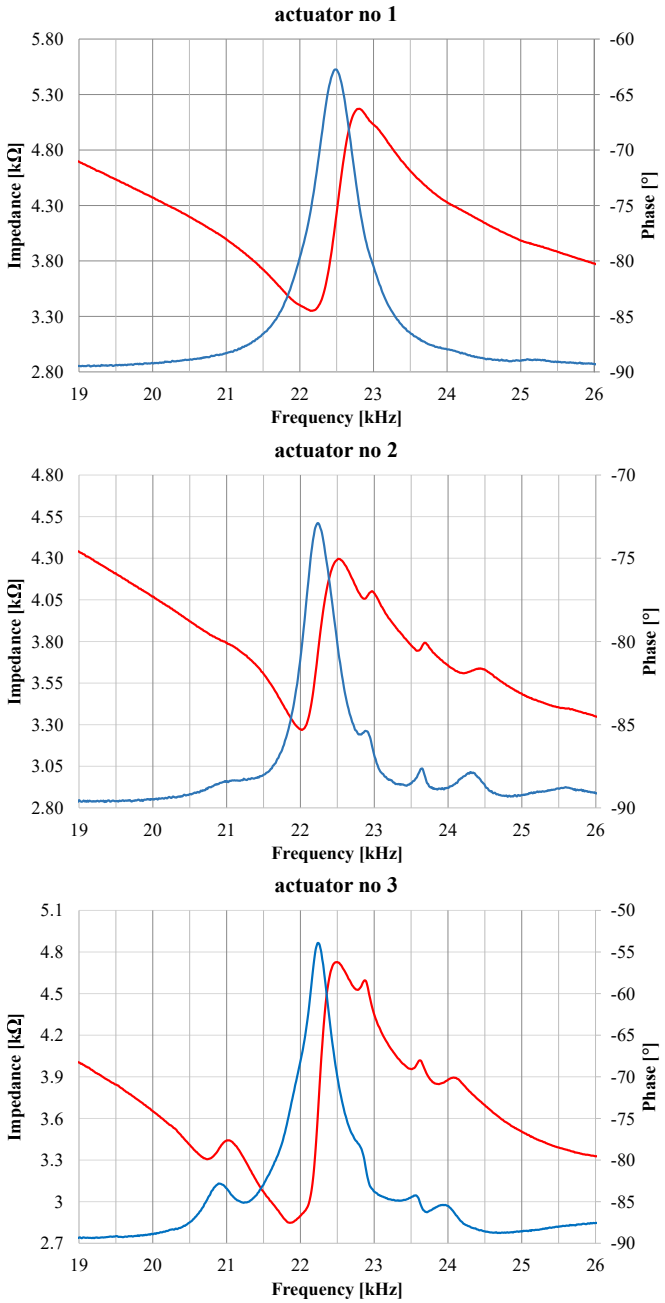

Fig. 14. Results of the resonance frequency measurements for each actuator, where the red line is impedance and the blue line is phase.

speed is in the range from 46 rpm to 48 rpm and the blocking torque is 0.4 Nm.

In the available literature one can find similar piezoelectric motors, which have the following parameters: maximum torque 0.06 Nm and maximum speed 65 rpm [22], maximum torque 0.08 Nm and maximum speed 250 rpm [6] and maximum torque 0.26 Nm and maximum speed 88 rpm [4]. Compared to the mentioned motors, the MPM prototype has a few times higher torque and lower speed. The authors tried to find a compromise between high blocking torque and maximum speed. Parameters of the MPM prototype can be considered sufficient in drives characterized by high torque and low speed.

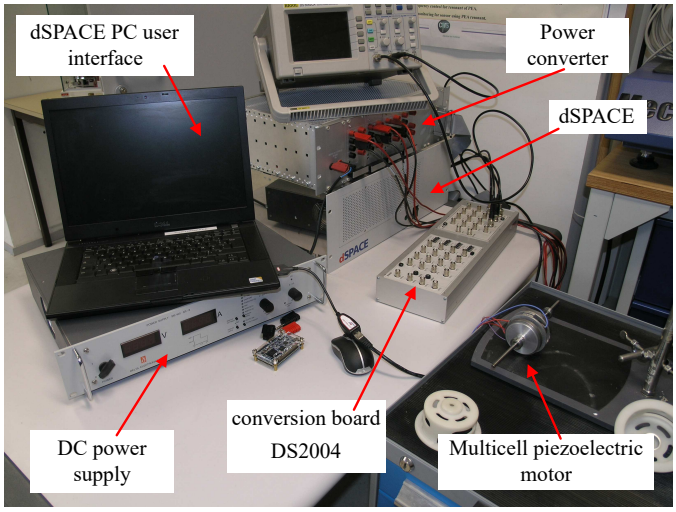

Fig. 15. The dSpace laboratory test bench at the Laboratory LAPLACE (INP-ENSEEIHT, Toulouse).

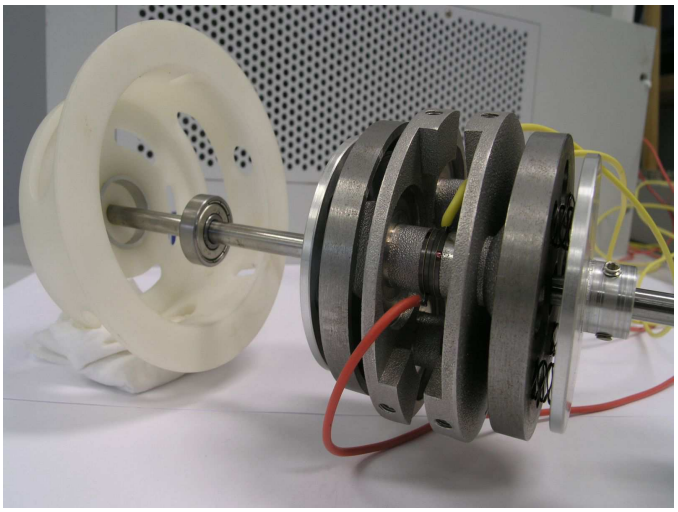

Fig. 16. The full assembly of the prototype of MPM.

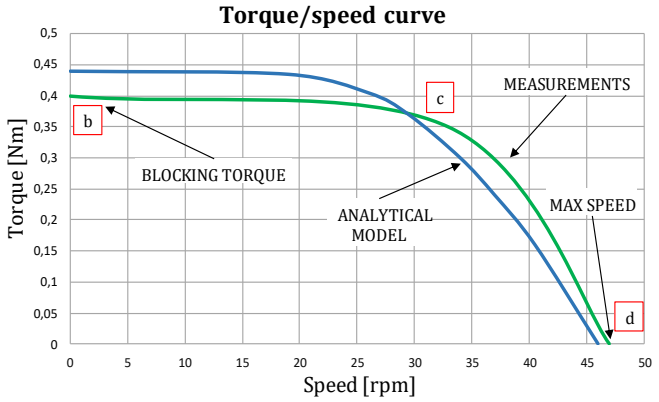

Fig. 17. Torque vs. speed characteristic of the prototype MPM.

VI. Conclusion

In this paper, the concept of a novel piezoelectric motor, referred to as a "multicell piezoelectric motor", has been presented. The MPM prototype consists of the following parts: the stator which consists of two pairs of piezoceramics and counter-masses with three rotating-mode actuators, two rotors, special springs, two ending plates and a shaft. The PZT piezoceramics are prestressed between two counter-masses. The FEM analysis has been carried out in the Autodesk environment (Multiphysics and Inventor) to determine the resonance frequencies and the stress in counter-mass structures. Moreover, the analytical model of the MPM has been developed and implemented in Matlab software to determine its torque vs. speed characteristics. Finally, the prototype has been manufactured and tested in the laboratory. The calculated values of blocking torque and speed were: 0.44 Nm and 47 rpm respectively. Moreover, the measurement results of the MPM were 0.4 Nm and 46-48 rpm. The FEM simulations gave a resonance frequency of about 25.6 kHz, and the measured resonance frequency was near 22 kHz for all three actuators. The results of FEA and analytical studies have been compared with measurement results. They have shown satisfying accuracy and provide useful perspectives for further MPM study and design. The developed analytical model of the MPM prototype can be used for preliminary analysis of motor properties and help to make design and manufacturing decisions.

Presently, the authors are working on a second MPM prototype motor with rotors made of glass-fiber and nylatron and a new counter-mass structure.

References

[1] C. H. Cheng and S. K. Hung, "A Piezoelectric Two-Degree-of-Freedom Nanostepping Motor With Parallel Design," *IEEE/ASME Transactions on Mechatronics*, vol. 21, no. 4, pp. 2197–2199, Aug. 2016.

[2] J. Li, X. Zhou, H. Zhao, M. Shao, N. Li, S. Zhang, and Y. Du, "Development of a Novel Parasitic-Type Piezoelectric Actuator," *IEEE/ASME Transactions on Mechatronics*, vol. 22, no. 1, pp. 541–550, Feb. 2017.

[3] T. Mashimo, S. Toyama, and H. Ishida, "Design and implementation of spherical ultrasonic motor," *IEEE Transactions on Ultrasonics, Ferroelectrics, and Frequency Control*, vol. 56, pp. 2514–2521, Nov. 2009.

[4] M. Hao and W. Chen, "Analysis and Design of a Ring-type Traveling Wave Ultrasonic Motor," in *2006 International Conference on Mechatronics and Automation*, Jun. 2006, pp. 1806–1810.

[5] L. Petit, R. Briot, L. Lebrun, and P. Gonnard, "A piezomotor using longitudinal actuators," *IEEE Transactions on Ultrasonics, Ferroelectrics, and Frequency Control*, vol. 45, no. 2, pp. 277–284, Mar. 1998.

[6] Y. Ting, Y. R. Tsai, B. K. Hou, S. C. Lin, and C. C. Lu, "Stator design of a new type of spherical piezoelectric motor," *IEEE Transactions on Ultrasonics, Ferroelectrics, and Frequency Control*, vol. 57, no. 10, pp. 2334–2342, Oct. 2010.

[7] L. Petit and P. Gonnard, "A multilayer TWILA ultrasonic motor," *Sensors and Actuators A: Physical*, vol. 149, no. 1, pp. 113–119, Jan. 2009. [Online]. Available: http://www.sciencedirect.com/science/article/pii/S092442470800513X

[8] T. Mashimo, "Piezoelectric rotational mixer based on a first bending vibration mode," *IEEE Transactions on Ultrasonics, Ferroelectrics, and Frequency Control*, vol. 60, no. 10, pp. 2098–2104, Oct. 2013.

[9] H. J. M. T. S. Adriaens, W. L. D. Koning, and R. Banning, "Modeling piezoelectric actuators," *IEEE/ASME Transactions on Mechatronics*, vol. 5, no. 4, pp. 331–341, Dec. 2000.

[10] K. Takemura and T. Maeno, "Design and control of an ultrasonic motor capable of generating multi-DOF motion," *IEEE/ASME Transactions on Mechatronics*, vol. 6, no. 4, pp. 499–506, Dec. 2001.

[11] "LAPLACE Laboratory on plasma and conversion of energy." [Online]. Available: http://www.laplace.univ-tlse.fr/?lang=en

[12] "Faculty Of Electrical And Control Engineering, Gdansk University of Technology." [Online]. Available: http://eia.pg.edu.pl/

[13] R. Ryndzionek, M. Ronkowski, M. Michna, . Sienkiewicz, and J. F. Rouchon, "Design, modelling and analysis of a new type of piezoelectric motor. Multicell piezoelectric motor," in *IECON 2013 - 39th Annual Conference of the IEEE Industrial Electronics Society*, Nov. 2013, pp. 3910–3915.
[14] R. Ryndzionek, M. Michna, M. Ronkowski, and J. F. Rouchon, "Analytical modelling of the multiceli piezoelectric motor based on three resonance actuators," in *IECON 2014 - 40th Annual Conference of the IEEE Industrial Electronics Society*, Oct. 2014, pp. 2701–2705.
[15] "Ultrasonic Motor - SHINSEI Corporation." [Online]. Available: http://www.shinsei-motor.com/English/techno/ultrasonic_motor.html
[16] W. Szlabowicz, "Contribution au dimensionnement et la ralisation d'actionneur pizolectrique rotation de mode fort couple pour application aronautique," Nov. 2006. [Online]. Available: http://ethesis.inp-toulouse.fr/archive/00000337/
[17] L. Petit and P. Gonnard, "Industrial design of a centimetric TWILA ultrasonic motor," *Sensors and Actuators A: Physical*, vol. 120, no. 1, pp. 211–224, Apr. 2005. [Online]. Available: http://www.sciencedirect.com/science/article/pii/S0924424704008325
[18] H. Hirata and S. Ueha, "Design of a traveling wave type ultrasonic motor," *IEEE Transactions on Ultrasonics, Ferroelectrics, and Frequency Control*, vol. 42, no. 2, pp. 225–231, Mar. 1995.
[19] M. Budinger, J. F. Rouchon, and B. Nogarede, "Analytical modeling for the design of a piezoelectric rotating-mode motor," *IEEE/ASME Transactions on Mechatronics*, vol. 9, no. 1, pp. 1–9, Mar. 2004.
[20] "Smalley steel ring company." [Online]. Available: https://www.smalley.com
[21] "Initial, Prodways Group." [Online]. Available: http://www.initial.fr/en
[22] S. x. Wu and C. Chen, "A dual ring rotary traveling wave ultrasonic motor," in *2016 Symposium on Piezoelectricity, Acoustic Waves, and Device Applications (SPAWDA)*, Oct 2016, pp. 176–180.

Roland Ryndzionek received the M.Sc. degree in electrical engineering in 2010 from the GUT, Poland and in 2012 M.Sc. from INP-ENSEEIHT Toulouse, France. He received a PhD degree from GUT and INP in 2015. From 2015 to 2017, he was a Postdoctoral Research Engineer in the SuperGrid Institute (Lyon, France) with the Power Electronics and Control Group. He is with GUT since 2017, currently as an Assistant Professor. His main scientific and research interests are electro-active materials, piezoelectric motors, designing of the mechatronic structures and power converters.

Michał Michna received the M.Sc., PhD, degrees in electrical engineering in 1999 and 2005, respectively, all from Gdansk University of Technology (GUT), Poland. He is with GUT since 1999, currently as an Assistant Professor. His main scientific and research interests cover a wide spectrum of mathematical modeling and diagnosis of electrical machines using analytical modeling and FEM-based computations. He is a Senior Member of the IEEE, New York.

Mieczysław Ronkowski received M.Sc., Ph.D. and D.Sc. degrees in Electrical Engineering from the Gdansk University of Technology (GUT), Poland, in 1969, 1979, and 1996, respectively. Since 1969, he has been on the staff of the GUT, presently holding the post of Associate Professor in the Chair of Power Electronics and Electrical Machines. In 1992 and 1993 he worked as a technical representative of the Vendor Surveillance Corporation (Irvine, California, USA) for the performance of quality engineering support tasks for the Energy Storage Inductor Project at the Scientific Industrial Association "URALELECTROTYAZHMASH" (Ekaterinburg, Russia). The Energy Storage Inductor Project was involved in the Superconducting Super Collider Laboratory Programme (Dallas, Texas, USA). In 1996, 1998, 1999, 2000, 2001, 2002, and 2003 he was invited for a stay as a visiting professor at the INP-ENSEEIHT, Toulouse, France. His current interests are focused on design, modeling (using field and circuit approaches) and testing of permanent magnet electrical machines (particularly machines for vehicle drives and wind generation systems), and piezoelectric motors. He is a member of the Polish Electrical Engineering Association, Poland, and member of the IEEE, New York.

Jean-Franois Rouchon received the Ph.D. degree in mechanical engineering from Ecole Centrale de Lyon (France) in 1996. Since 1998 he has been with the Laboratory of Plasma and Energy Conversion (Laplace), Toulouse, France and Ecole Nationale Suprieure d'Electrtechnique, d'Electronique, d'Informatique, d'Hydraulique et des Télécommunications (ENSEEIHT). Since 2015, Jean-Franois Rouchon is the director of the INP-ENSEEIHT. Jean-Franois Rouchon research is developed within the Electrodynamic - GREM3 research team, in the field of electromechanical energy conversion. His activities are focused on the development of piezoelectric motors for embedded applications, tribology of contact and design of electro-active structures for sensing and measurement.